www.czasopisma.pan.pl PAN POLSKA AKADEMIA NAUK www.journals.pan.pl

Arch. Metall. Mater. **68** (2023), 2, 649-658

DOI: https://doi.org/10.24425/amm.2023.142446

HAIJIAN XU[1,2*], CHUFEI HAN[2], PINGYUAN YAN[2], BAOCHUN ZHAO[2], WEIJUAN LI[1*]

EFFECT OF COOLING RATES AND INTERMEDIATE SLAB BLANK THICKNESS ON THE MICROSTRUCTURE AND MECHANICAL PROPERTIES OF THE X70 PIPELINE STEEL

In this study, the microstructures and mechanical properties of X70 pipeline steels produced with varying Mo contents, accelerated cooling rate and intermediate slab blank thickness are systematically investigated. Results showed that the microstructures and mechanical properties of the X70 pipeline steels were strongly affected by Mo addition. The pearlite and proeutectoid ferrite formation is obviously inhibited in containing-Mo steel and the acicular ferrite (AF) is obtained in a wide range of cooling rates. With the increasing the cooling rates, the AF constituent amount increases. The grains can be refined by increasing the thickness of intermediate slab for enhancing the cumulative reduction rates, and meanwhile increase the number density of precipitates. It was proved by simulation and industrial trials that the low-alloy X70 pipeline steels can be produced increasing cooling rates and the thickness of intermediate slab without strength and toughness degradation which also reduce alloy cost.

Keywords: cooling rate; microstructure; pipe steel; acicular ferrite; low-alloy

1. Introduction

Pipeline steels used to transport oil or gas are critical due to continually growing demand in energy. The transmission environment is becoming complicated and the delivery pressure is increasing. In modern pipeline design standard, high strength and good toughness are the most common requirements for high level pipeline steels (X70-X100 grades) in order to improve the transportation efficiency [1-6]. High strength means cost reductions by decreasing the plate thickness and production costs which seems to enhance transportation efficiency [7,8]. Under the condition of reduced toughness, the improvements in strength are easy to achieve, while toughness is an imperative property to ensure the safety of service, especially operate in extreme environmental such as earthquake-prone areas [9,10]. In order to improve the strength and toughness of the pipeline steels, the design of composition together with suitable thermo-mechanical controlled processing (TMCP) achieve the ideal microstructures, and through them enhancing mechanical properties [11-13]. In order to obtain the properties requirements, the traditional high-grade pipeline steels need more expensive microalloying elements additions (Ni, Mo, Nb and Ti) for promoting the acicular ferrite and bainite formation, and precipitation strengthening [14,15]. However, the alloys Mo, Ni are very expensive, and the addition of these microalloying elements will obviously increase the production cost.

It is well understood that TMCP parameters are the main manufacturing technology in controlling the mechanical properties of high-grade pipeline steels. The properties are mainly dependent on the chemical composition, slab heating temperatures, reduction ratio in the different rolling regions, rolling temperatures and the cooling rate et al. [14-20]. These parameters strongly affect the microstructure evolution and mechanical properties. Some groups have found that different levels of Mo addition had a remarkable effect on the microstructures and mechanical properties of the X80 grade pipeline steels [21]. The appropriate microstructure for low carbon high strength steels are formed at low transformation temperatures as non-equilibrium, non-equiaxed structures like very low carbon acicular ferrite which contain high dislocation densities and precipitates for achieving an optimum combination of strength and high toughness [22-24]. Compared to a microstructure of polygonal ferrite, acicular ferrite contains higher density of dislocations and sub-boundaries, which is beneficial to the strength and toughness [16]. Acicular ferrite is usually composed of nonparallel ferrite laths with high number density of dispersed

[1] SCHOOL OF MATERIALS AND METALLURGY, UNIVERSITY OF SCIENCE AND TECHNOLOGY LIAONING, ANSHAN, 114051, P.R. CHINA
[2] ANGANG STEEL COMPANY LIMITED, ANSHAN, 114009, P.R. CHINA

* Corresponding author: haijianxu2013@163.com

precipitation of carbonitrides. The acicular ferrite provides a continuous yielding phenomenon and rapid work hardening during the fabrication pipes [22,24-26]. Up to now, the acicular ferrite forms through a mixed diffusion or shear mechanism during continuous cooling after hot rolling. The temperature range slightly is above bainite and usually nucleates on dislocations or other defects within the grains. In pipeline steels, an increase in the amount of finish rolling in the austenite non-recrystallization región during deformation increases the volume fraction of acicular ferrite after cooling at the expense of bainitic and ferrite [22,25-27]. The total deformation degree of roughing and especially the final deformation passes have a great influence on the toughness and strength.

Up to now, the mechanical properties of alloy reduction can be improved by using ultra fast cooling process on the new generation thermo-mechanical-controlled processing (NG-TMCP) [21]. However, it needs extra investment in the equipment aspects. We can make full use of the advantage of precipitates strengthening, grain refinement and optimize the rolling parameters for solving this problem. In addition, the effect of intermediate slab blank thickness on the microstructure of X70 grade pipe steels require further systematically investigation.

Therefore, the goal of the present work was to investigate the microstructure of X70 pipeline steels with different Mo contents and cooling rates in the laboratory. On the other hand, the evolution of precipitation states, grain characteristic and mechanical properties with different intermediate slab blank thickness are also described in this paper. On the basis of above research, the effect of cooling rates intermediate slab blank thickness on alloy cost reduction X70 pipe steels was verified by an industrial trial.

2. Experimental

The investigated steels were industrial API 5L X70 type pipeline steels containing different levels of Mo. The actual chemical compositions are shown in TABLE 1. The minor difference for the steels is the Mo contents. The cylindrical compression samples of 15 mm in height and 8 mm in diameter were fabricated from the billet. Thermo-mechanical processing simulations were isothermally compressed on a thermal-mechanical simulator Gleeble-3800. Specimens were heated to 1200°C at the rate of 10°C/s and then kept for 300s to homogenize the microstructure, and then cooled to 860°C and held for 30s to eliminate the thermal gradient before the compression tests. The true strain was 0.4 and the deformation rate was $10s^{-1}$. After compression, the specimens were cooled to room temperature at different rates (1, 5, 10, 15, 20, and 30°C/s). The thermal simulation procedure on the specimens is shown in Fig. 1. An overall intermediate slab blank thickness effect was expected by rolling with a high rolling reduction ratio (over 75%) in the non-recrystallized region of austenite after austenitization at 1120°C in X70M pipeline steel. The intermediate slab blank thickness was 50 mm, 60 mm and 70 mm, respectively. Rolling was finished in the range of Ar_3+60°C, which were the temperature of austenite single phase region, to produce two steel plates. The accelerated cooling exit temperature was 400°C with the cooling rate 15°C/s.

TABLE 1

Chemical composition of the X70 pipeline steels with different Mo contents (wt%)

Steel	C	Si	Mn	P	S	Cr	Nb	Ti	Mo
ST1	0.054	0.23	1.62	0.012	0.008	0.20	0.05	0.015	0
ST2	0.053	0.23	1.63	0.011	0.008	0.19	0.05	0.015	0.04
ST3	0.053	0.22	1.62	0.012	0.008	0.19	0.05	0.014	0.08

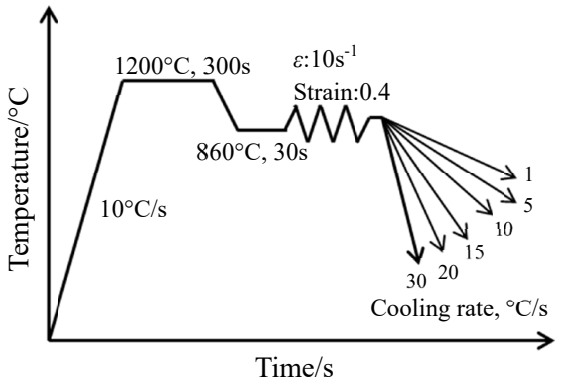

Fig. 1. Thermal simulation procedure of the X70 pipeline steel

The deformed specimens in different status for microstructure characterization were cut parallel to the compression axis at geometric center or the middle of plates along transverse direction with full thickness. Specimens for optical and scanning electron microscopy (SEM) observations were mechanically polished and etched in a 4% nital solution. The microstructure evolution in X70 pipeline steel with different intermediate slab blank thickness was determined using by Electron backscattered diffraction (EBSD) with a step size of 0.8 μm and transmission electron microscopy (TEM). The EBSD specimens were mechanical polished and then electro-polished by electrolytic polishing with 10%$HClO_4$+90%ethanol solution in order to remove the deformation layer introduced during mechanical milling. TEM specimens were prepared by using the extraction replica technique. The precipitates extracted from ϕ3 mm disks of the X70 pipeline steels were retrieved in a thin carbon film. The procedures for the preparation are as follows: ϕ3 mm disks mechanically polished were pre-etched in a dilute acid solution (10%$HClO_4$+90%ethanol) for 5 min. The chemically etched surfaces were then coated with an amorphous carbon film to a thickness of about 1200Å, and subsequently chemically etched again in a similar acid solution to make the separation of carbon films from the substrate of the steel disks. The floating carbon films, after cleaned carefully in an ethanol solution, were finally retrieved on some ϕ3 mm copper meshes.

The tensile specimens were cut from the rolled plates in the transverse direction. The dimension of tensile specimens is 12.7 mm in diameter and 50.8 mm in length. Tensile tests were

conducted at room temperature at a cross-head speed of 5 mm/min. The drop weight tear test (DWTT) specimens were machined into the dimensions of 75×22×305 mm^3 (T-L). The DWTT test temperatures were performed at –15°C. Full size Charpy impact specimens were machined from the hot-rolled plates in the transverse direction with their notch parallel to the rolling direction (T-L), and impact tests were performed at –20°C.

3. Results

3.1. Microstructures evolution with different cooling rates

Fig. 2 shows OM in the ST1 specimen without Mo addition cooled at different rates. When the cooling rate was less than 15°C/s, the microstructures were composed of polygonal ferrite (PF) and pearlite (P). As the cooling rate increased, polygonal ferrite content decreased, and the acicular ferrite content increased. When the cooling rate increased to 20°C/s, the polygonal ferrite transformation was reduced and acicular ferrite and bainite became the dominant feature. When the cooling rate was further increased, microstructures became more refined. After the continuous cooling simulation was completed, the collected expansion-temperature curves were plotted to determine phase transition points.

Fig. 3 shows the optical micrographs (OM) of the ST2 specimen cooled at different rates. It can be seen that when the cooling rate was less than 10°C/s, the microstructures were mainly composed of polygonal ferrite and pearlite. When the cooling rate was larger than 20°C/s, the acicular ferrite (AF) and granular bainite (GB) was the dominant microstructure component with the increasing cooling rate. Fig. 4 shows the optical micrographs (OM) of the ST3 specimen cooled at different rates. It can be seen

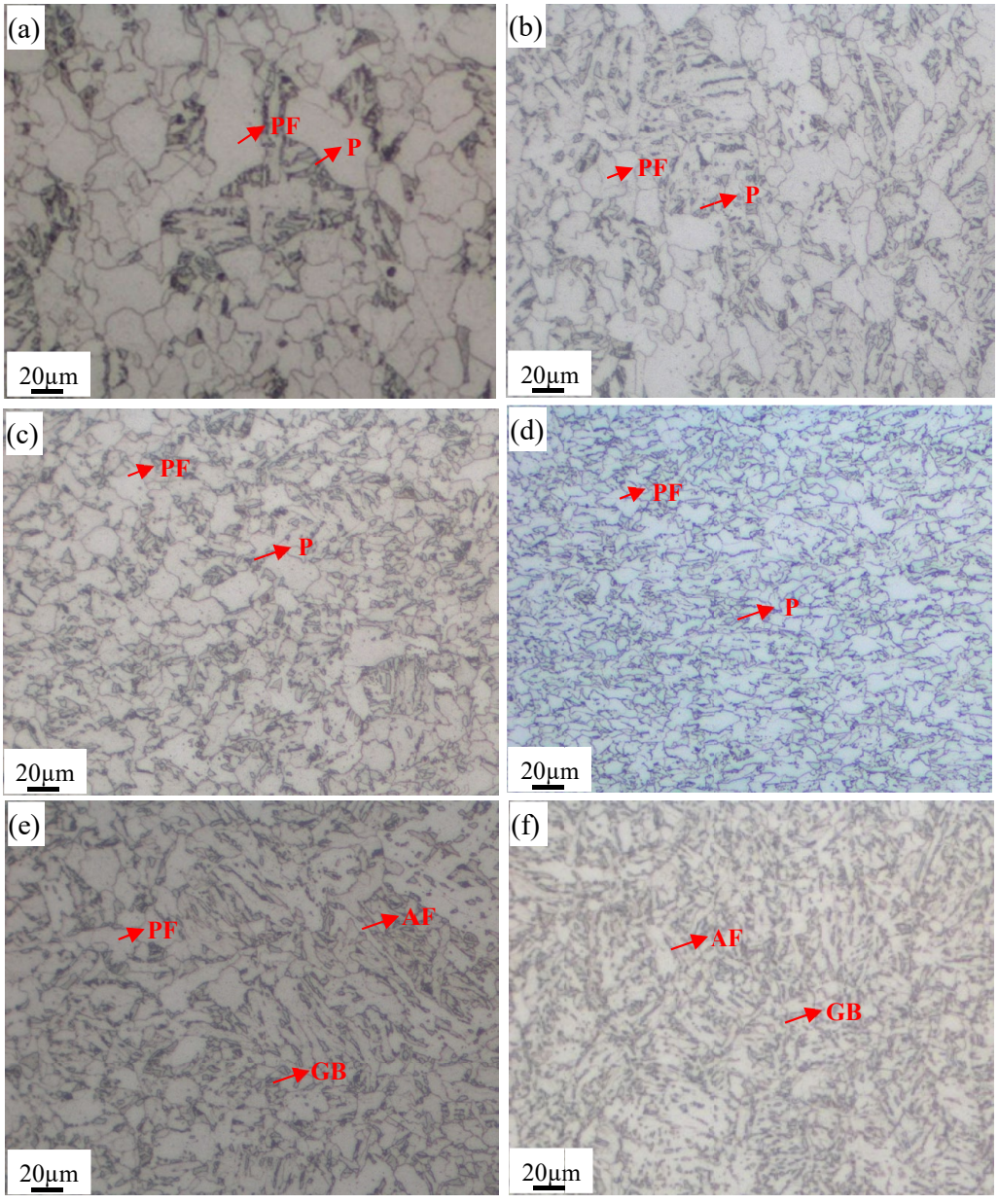

Fig. 2. Optical micrographs in the ST1 specimen cooled at different rates. (a) 1°C/s, (b) 5°C/s, (c) 10°C/s, (d) 15°C/s, (e) 20°C/s, (f) 30°C/s

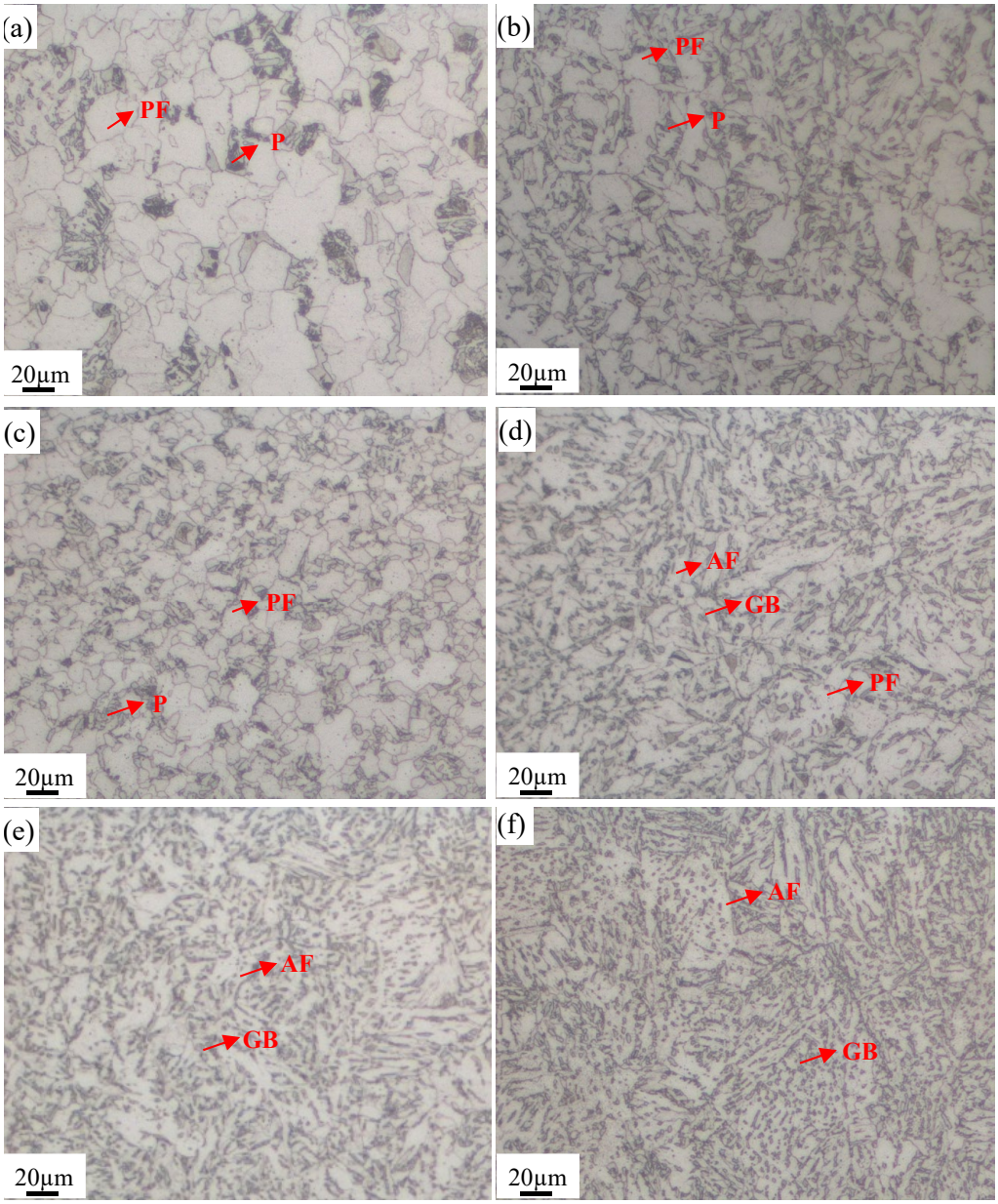

Fig. 3. Optical micrographs in the ST2 specimen cooled at different rates. (a) 1°C/s, (b) 5°C/s, (c) 10°C/s, (d) 15°C/s, (e) 20°C/s, (f) 30°C/s

that when the cooling rate was less than 5°C/s, the microstructures were mainly composed of polygonal ferrite and pearlite. When the cooling rate was larger than 15°C/s, the acicular ferrite (AF) and bainite was the dominant microstructure component with the increasing cooling rate. When the cooling rate was further increased to 30°C/s, the large quantity of granular bainite microstructures became the dominant microstructure. The measured Ar_3 is 895°C, 898°C and 903°C with the increasing the Mo content according to the calculation following equations Ar_3 = 937.2–436.5C+56Si–19.7Mn+4.9Cr+38.1Mo+136.3Ti–19.1Nb [28]. It can be inferred that the Mo addition could improve the stability of austenite and hinder the formation of proeutectoid ferrite (polygonal ferrite) and pearlite. Therefore, acicular ferrite was obtained over a wide range of cooling rates. However, polygonal ferrite was formed over a wider range of cooling rates and pearlite was also formed at lower cooling rates in the ST1 specimen.

3.2. Effect of the intermediate slab blank thickness on the microstructures and mechanical properties

Fig. 5 shows the results of metallographic analysis obtained by SEM. It is demonstrated, that the intermediate slab blank thickness of 50 mm provides microstructure, consisting mainly of quasi polygonal ferrite and small amount globular bainite (GB). With the increasing the intermediate slab blank thickness, the microstructure mainly consist of AF and GB. Due to this, microstructure gets more refined. These effects were also observed in similar studies [22].

Fig. 6a and b shows the grain boundaries maps for ST3 specimens with different intermediate slab blank thickness. It can be seen that very similar results were obtained from SEM results. In addition, there were high densities of HAGBs (red lines) in the AF; in contrast, it was few in PF. With the increase

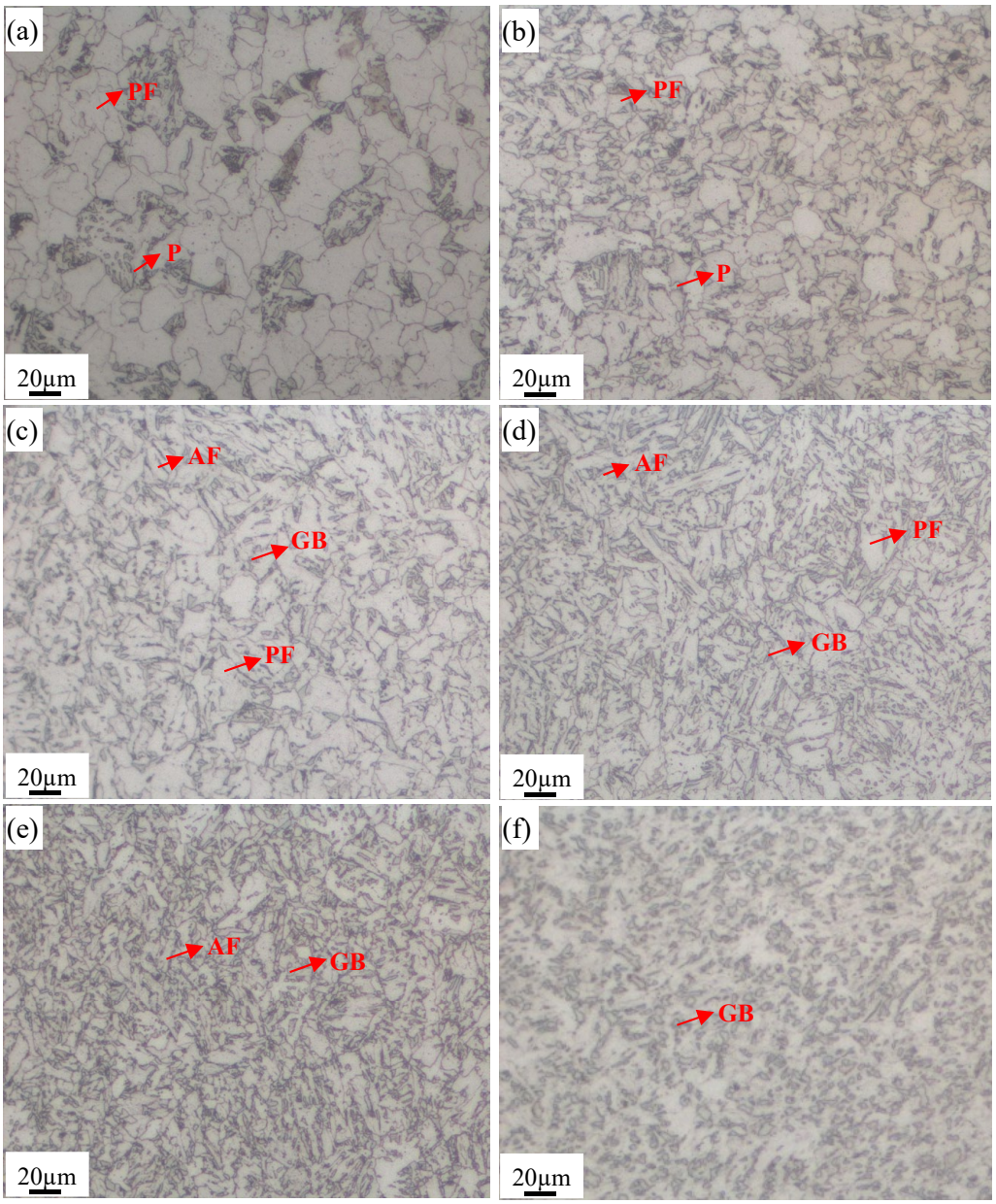

Fig. 4. Optical micrographs in the ST3 specimen cooled at different rates. (a) 1°C/s, (b) 5°C/s, (c) 10°C/s, (d) 15°C/s, (e) 20°C/s, (f) 30°C/s

in intermediate slab blank thickness, the content of AF varied significantly. In the 60 mm thickness, PF was dominant with less BF (≈35% in volume fraction). In the 70 mm thickness, the content of AF was greatly to 60% at the expense of PF. Fig. 6c shows the histogram of misorientations with different intermediate slab blank thickness in the specimens. In the 60 mm thickness, the proportion of HAGBs (black lines) was about 38% and the average grain size was 7.35 μm. In the 70 mm thickness, the proportion of HAGBs increased to 68%, whereas the average grain size decreased to 3.78 μm. The finer grain size and higher fraction of HAGBs can strongly hinder the fracture propagation and decrease the ductile-brittle transition temperature.

The morphologies of the extracted precipitates formed at different intermediate slab blank thickness are shown in Fig. 7a and b. The increase in the intermediate slab blank thickness has a great effect on the average size and number density of precipitates. These led to a decrease in the frequency of the largest precipitates (>20 nm) and an increase in the frequency of the smallest precipitates (<20 nm). The average size is 18.2 nm and 13.1 nm in the intermediate slab blank thickness of 60 nm and 70 nm, respectively. High resolution transmission electron microscope (HRTEM) imaging was performed to identify the crystal structure of these precipitates in the 70 mm intermediate slab blank thickness with different size. According to the statistic results of HRTEM analyses, HRTEM and its FFT filtered image was performed to determine the crystalline structure of these big precipitates (diameter, 60 nm), as shown in Fig. 8. The lattice structure of these precipitates from the image is in good agreement with cubic structure Ti_2N with zone axis of [0 1 0]. The two measured atomic planes are indexed as (0 0 4) and (2 0 0), respectively. Fig. 9 shows an HRTEM lattice image of these small precipitates (diameter, 15nm), its fast fourier transform

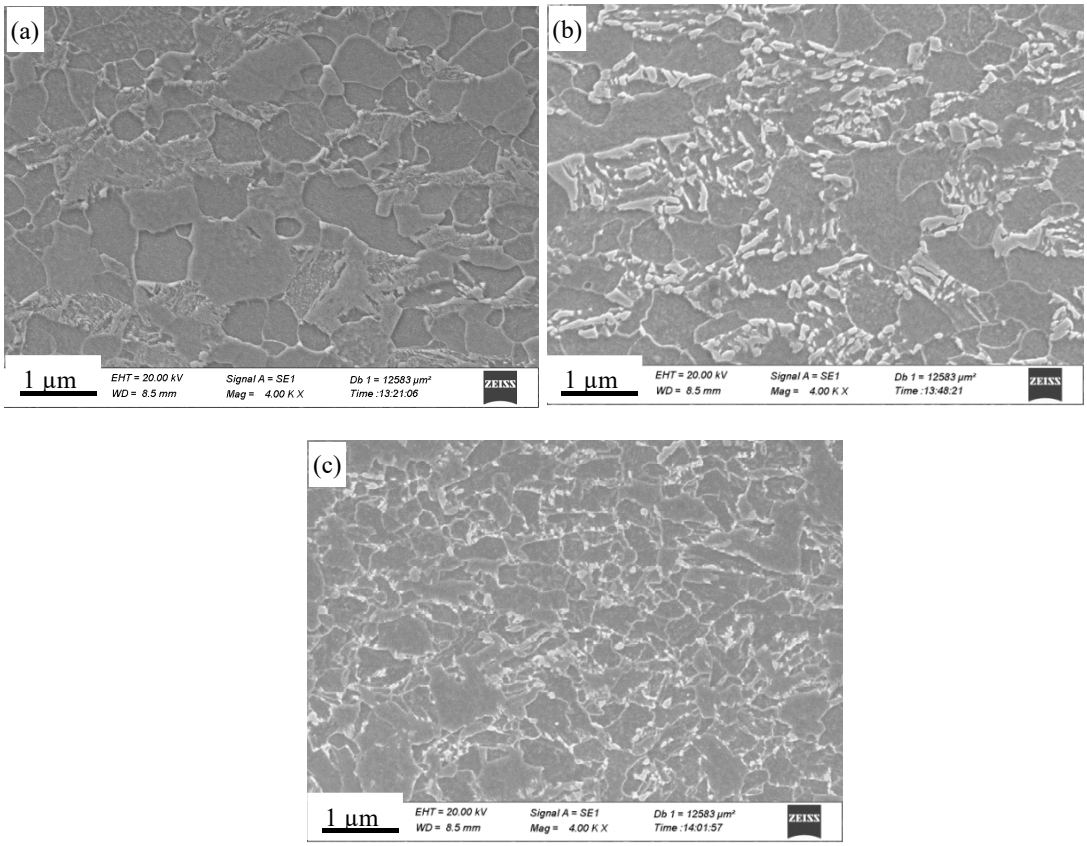

Fig. 5. Effect of intermediate billet thickness on microstructure of X70M pipeline steel. (a) 50 mm, (b) 60 mm, (c) 70 mm

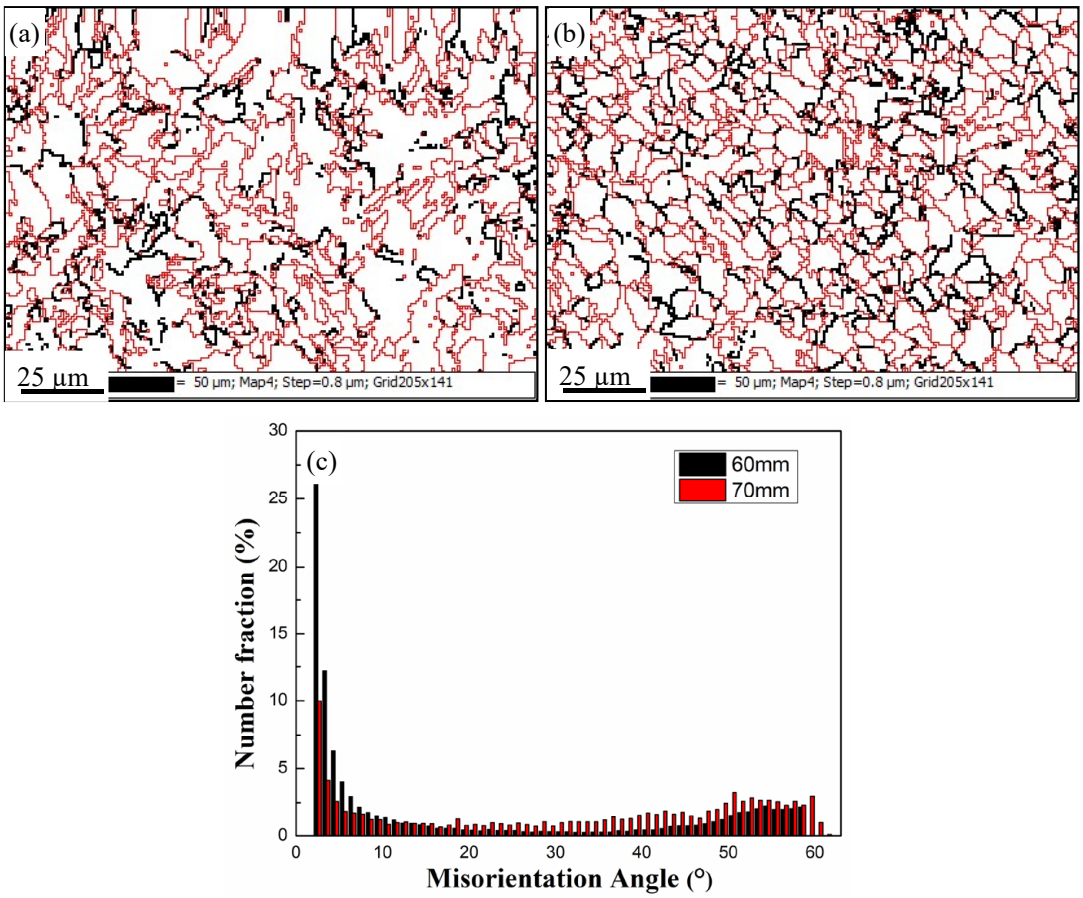

Fig. 6. Grain boundary maps with different intermediate billet thickness (LAGBs 2-15° and HAGBs >15° indicated by red and black lines). (a) 60 mm, (b) 70 mm, (c) Histogram of misorientation

(FFT) image and FFT filtered image with an incident electron is parallel to the [0 1 –1] zone axis. Two measured atomic plane distances are 2.55Å and 2.21Å with an angle of 56°. This result is in good agreement with the cubic structure NbC.

The measured mechanical properties with different intermediate slab blank thickness are shown in TABLE 2. It is seen that different intermediate slab blank thickness has a strong effect on the mechanical properties. It can be concluded that the refinement of grain and precipitates could improve mechanical properties with increasing the intermediate slab blank thickness, which satisfied the requirements of X70 pipeline steel.

TABLE 2

Comparasion of mechanical properties obtained with different intermidiate slab thickness of X70 pipeline steels

Intermediate slab blank thickness /mm	*Rp*0.2 /MPa	R_m /MPa	–15°CA_{kv2} /J	–15°CDWTT%
50	486	572	201	85
60	503	588	213	88
70	528	612	245	92
Standard	485-635	570-760	≥150	≥85

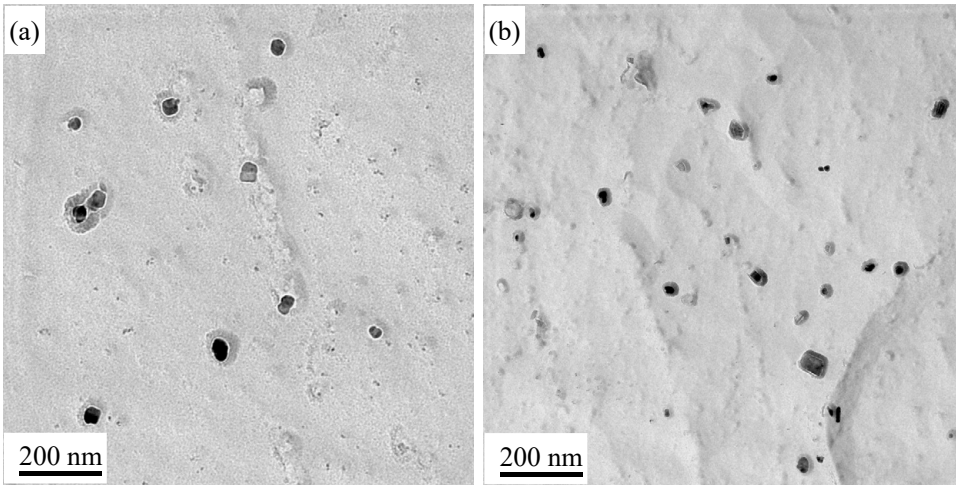

Fig. 7. Morphologies of precipitates with different intermediate billet thickness. (a) 60 mm, (b) 70 mm

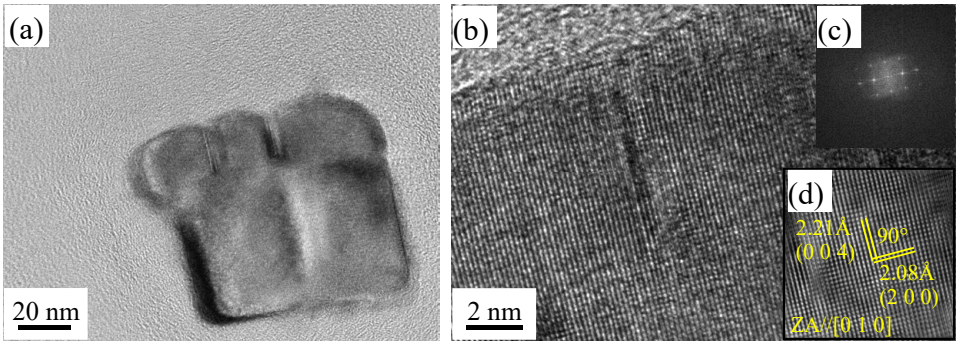

Fig. 8. TEM analysis of Ti_2N precipitates. (a) Bright field, (b) HRTEM images of precipitates, (c) FFT diagram of the micrographs in (b), (d) FFT filtered images derived from the images (b)

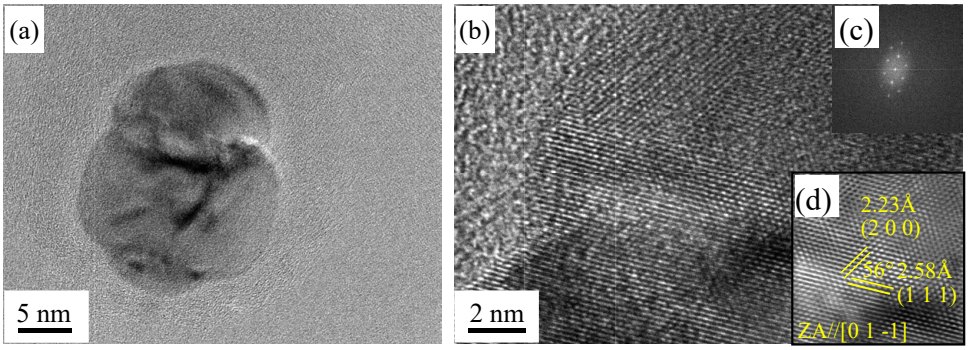

Fig. 9. TEM analysis of NbC precipitates. (a) Bright field, (b) HRTEM images of precipitates, (c) FFT diagram of the micrographs in (b), (d) FFT filtered images derived from the images (b)

4. Discussion

4.1. Effect of Mo on the microstructures

By comparing microstructures (Fig. 2-Fig. 4) in the X70 pipeline steel with different Mo contents, it was found that Mo addition could expand the region of AF formation regions and hinder the formation of proeutectoid ferrite (polygonal ferrite) and pearlite at low cooling rate. Owing to the scientific research and save the production cost, several groups have carried out on the effect of Mo addition on the γ-α transformation [29]. The formation of proeutectoid ferrite were postponed and suppressed by Mo addition. At immediate temperatures, the steels with Mo addition own a deep bay [30]. The above phenomenons are may attributed to the segregation of Mo atoms at γ/α boundaries. The boundaries collect large quantity of Mo atoms during the transformation. As a result, Mo atoms experience an impurity drag or solute drag [31,32]. The Mo elemental accumulated at γ/α boundaries below the TTT-diagram bay could be reduced by deformation due to the solute drag effect [33]. AF is an intermediate temperature-transformed phase, which also called intragranularly nucleated bainite [34]. Therefore, the formation of proeutectoid ferrite was suppressed due Mo addition by promoting the formation of AF and bainite. Otherwise, the nucleation and growth rate of the pearlite were also affected by Mo addition [35]. The Mo elemental addition strongly inhibits pearlite formation. On the contrary, the pearlite reaction only occurred when the austenite was refined and severely deformed [33]. Base on the above analysis, in order to ensure the properties of X70 pipeline steel without Mo addition, the cooling rate should be increased by avoiding the formation of proeutectoid ferrite (polygonal ferrite) and pearlite areas. Otherwise, Al deoxidation is used in pipeline steel. Some specific Al_2O_3 non-metallic inclusions could promote AF nucleation at these non-metallic inclusions [34].

4.2. Effect of intermediate slab blank thickness on the Microstructures

By comparing microstructures (Fig. 5, 6 and 7) and mechhaical properties (TABLE 2) in the ST3 specimen, it can be seen that strength and toughness values are the function of the intermediate slab blank thickness. Thus, with the increasing of the intermediate slab blank thickness, the tensile strength, Charpy V-notch impact energy and DWTT values increases. This effect is associated with refinement of grain size and increased content of AF. Moreover, its precipitates and grain size become finer and the number density of precipitates are higher. This is because of the high stored energy introduced by increasing the cumulative reduction rates that led to the decreased activation energy for nucleation and increased driving force for precipitation in addition to the increased diffusion rate of the microalloying elements in the strained austenite due to the formation of a larger amount of AF. The strain-induced Nb(C, N) precipitation exist in the pipeline steels. The Nb(C, N) precipitated in austenite, which impedes the growth of the recrystallization of austenite grains. It promotes austenite grain refinement. Otherwise, it also increases the dislocation density of austenite, which is beneficial for the formation of sub-grain boundary of the deformed austenite [2]. In addition to the prior austenite grain boundaries, the new introduced subgrain boundaries and dislocations as a result of deformation led to the increasing nucleation sites and the kinetics of precipitation through pipe diffusion along with dislocation core [35]. Similar results were also obtained in in the Nb-Ti-bearing high-strength low-alloy steel [36]. The precipitation kinetics in this low-alloy steel is accelerated in deformed austenite compared with undeformed austenite and becomes more significant with the decreasing deformation temperature.

The precipitates formed in the deformed austenite were also finer than those formed in the undeformed austenite. The finer precipitates lead to a increase in the grain boundary pinning effect, and refine the grain size. This increases the grain boundary pinning effect, thereby retaining a finer recrystallized austenite grain size at this stage of the forging process. As far as grain size was concerned, it decreased significantly with the increasing the cumulative reduction rates. The formation temperature of AF was higher, and the misorientation between different AF and bainite was big. Thus, it was rather to form higher ratio of HAGBs than origin LAGBs. In the industry production, The two principles of conventional-accelerated continuous cooling (ACC) still insist on the conventional TMCP, namely the control of austenitic hardening and the phase transformation of the austenite. Therefore, ACC plays an important role in improving the microstructure and mechanical properties by grain refinement. The steel was still in the state of non-recrystallization in a very short time after hot deformation with a large number of "defects". It promote the nucleation for the phase transformation. Owing to the implementation of ACC, the cooling rate between 15-30°C ensured passing through the austenite region in a very short time, which results in hardened austenite before phase transformation. The hardened austenite was beneficial to refine the transformed steel plates. Therefore, it is important to adjust the cooling rates in controlling the microstructure, which depends on the Mo contents.

5. Conclusions

This research addresses the effect of thermo-mechanical treatment with different cooling rates and intermediate billet thickness on the microstructure and mechanical properties of the X70 pipeline steels. The results can be summarized as follows:

(1) The hot simulation experiment showed that Mo content had obvious influence on the microstructure of the X70 pipeline steel. In the high-Mo steel, AF was obtained within a wide range of cooling rates owing to the inhibition of polygonal ferrite and pearlite. In the low-Mo steel, the dominant AF microstructure could be obtained only when the cooling rates reached up to 20°C/s.

(2) With the increase in the intermediate billet thickness from 60 mm to 70 mm, the proportion of HAGBs significantly increased from 38% to 68%, accompanied with the decrease in average grain size from 7.35 to 3.78 μm. Otherwise, the content of AF was greatly to 60% at the expense of PF in the 70 mm thickness. The increase the intermediate slab blank thickness could refine the average size and increase the number density of precipitates.

(3) The improvement of microstructure could enhance the mechanical properties with increasing the intermediate slab blank thickness, which satisfied the requirements of X70 pipeline steel.

Acknowledgments

This research is supported by the China Postdoctoral Science Foundation funded project (2018M641699).

REFERENCES

[1] C.U. Jeong, W. Woo, J.Y. Choi, S.H. Choi, Effect of kinematic stability of initial orientation on deformation heterogeneity and ductile failure in duplex stainless steel during uniaxial tension, Acta. Mater. **67**, 21-31 (2014). DOI: https://doi.org/10.1016/j.actamat-2013-020

[2] F. Zanotto, V. Grassi, A. Balbo, C. Monticelli, F. Zucchi, Stress corrosion cracking of LDX 2101 duplex stainless steel in chloride solutions in the presence of thiosulphate, Corros. Sci. **80**, 205-212 (2014). DOI: https://doi.org/10.1016/j.corsci-2013-028

[3] J. Xiong, M.Y. Tan, M. Forsyth, The corrosion behaviors of stainless steel weldments in sodium chloride solution observed using a novel electrochemical measurement approach, Desalination **327**, 39-45 (2013). DOI: https://doi.org/10.1016/j.desal-2013-08-006

[4] S. Spigarelli, M.E. Mehtedi, P. Ricci, C. Mapelli, Constitutive equations for prediction of the flow behaviour of duplex stainless steels, Mater. Sci. Eng. A. **527** (16-17), 4218-4228 (2010). DOI: https://doi.org/10.1016/j.msea-2010-03-029

[5] M.L. Angelescu, E.M. Cojocaru, N. Serban, V.D. Cojocaru, Evaluation of Hot Deformation Behaviour of UNS S32750 Super Duplex Stainless Steel (SDSS) Alloy, Metals **10** (5), 10050673 (2020). DOI: https://doi.org/10.3390/met-10050673

[6] J.O. Nilsson, Super duplex stainless steels, Mater. Sci. Technol. **8**, 685-700 (1992). DOI: https://doi.org/10.1179/mst-1992-8-8-685

[7] A. Iza-Mendia, A. Piñol-Juez, J.J. Urcola, I. Gutierrez, Microstructural and mechanical behavior of a duplex stainless steel under hot working conditions, Metall. Mater. Trans. A. 29, 2975-2986 (1998). DOI: https://doi.org/10.1007/s11661-998-0205-z

[8] D.N. Zou, K. Wu, Y. Han, W. Zhang, B. Cheng, G.J. Qiao, Deformation characteristic and prediction of flow stress for as-cast 21Cr economical duplex stainless steel under hot compression,, Mater. Des. 51, 975-982 (2013). DOI: https://doi.org/10.1016/j.matdes-2013-04-065

[9] J.H. Kang, S.J. Heo, J. Yoo, Y.C. Kwon, Hot working characteristics of S32760 super duplex stainless steel, J. Mech. Sci. Technol. **33**, 2633-2640 (2019). DOI: https://doi.org/10.1007/s12206-019-0511-y

[10] Y. Fang, Z. Liu, G. Wang, Crack Properties of Lean Duplex Stainless Steel 2101 in Hot Forming Processes, J. Iron. Steel. Res. Int. **18**, 58-62 (2011). DOI: https://doi.org/10.1016/S1006-706X(11)60051-4

[11] Y.L. Fang, Z.Y. Liu, H.M. Song, L.Z. Jiang, Hot deformation behavior of a new austenite-ferrite duplex stainless steel containing high content of nitrogen, Mater. Sci. Eng. A, **526** (1-2), 128-133 (2009). DOI: https://doi.org/10.1016/j.msea.2009-07-012

[12] S. Wronski, J. Tarasiuk, B. Bacroix, A. Baczmanski, C. Braham, Investigation of plastic deformation heterogeneities in duplex steel by EBSD, Mater. Charact. **73**, 52-60 (2012). DOI: https://doi.org/10.1016/j.matchar.2012-07-016

[13] R. Dakhlaoui, A. Baczmanski, C. Braham, S. Wronski, K. Wierzbanowski, E.C. Oliver, Effect of residual stresses on individual phase mechanical properties of austeno-ferritic duplex stainless steel, Acta Mater. **54** (19), 5027-5039 (2006). DOI: https://doi.org/10.1016/j.actamat.2006-06-035

[14] Y. Han, D.N. Zou, Z.Y. Chen, G.W. Fan, W. Zhang, Investigation on hot deformation behavior of 00Cr23Ni4N duplex stainless steel under medium-high strain rates, Mater. Charact. **62** (2), 198-203 (2011). DOI: https://doi.org/10.1016/j.matchar.2010-11-013

[15] M. Faccoli, R. Roberti, Study of hot deformation behaviour of 2205 duplex stainless steel through hot tension tests, J. Mater. Sci. **48**, 5196-5203 (2013). DOI: https://doi.org/10.1007/s10853 -013-7307-8

[16] O. Balancin, W.A.M. Hoffmann, J.J. Jonas, Influence of microstructure on the flow behavior of duplex stainless steels at high temperatures, Metall. Mater. Trans. A, **31**, 1353-1364 (2000). DOI: https://doi.org/10.1007/s11661-000-0254-4

[17] N. Haghdadi, P. Cizek, H. Beladi, P.D. Hodgsn, A novel high-strain-rate ferrite dynamic softening mechanism facilitated by the interphase in the austenite/ferrite microstructure, Acta. Mater. **126**, 44-57 (2017). DOI: https://doi.org/10.1016/j.actamat.2016-12-045

[18] Y.Y. Liu, H.T. Yan, X.H. Wang, M. Yan, Effect of hot deformation mode on the microstructure evolution of lean duplex stainless steel 2101, Mater. Sci. Eng. A. **575**, 41-47 (2013). DOI: https://doi.org/10.1016/j.msea.2013-03-036

[19] G.W. Fan, J. Liu, P.D. Han, G.J. Qiao, Hot ductility and microstructure in casted 2205 duplex stainless steels, Mater. Sci. Eng. A. **515** (1-2), 108-112 (2009). DOI: https://doi.org/10.1016/j.msea.2009-02-022

[20] G. Fargas, M. Anglada, A. Mateo, Effect of the annealing temperature on the mechanical properties, formability and corrosion resistance of hot-rolled duplex stainless steel, J. Mater. Process. Technol. **209** (4), 1770-1782 (2009). DOI: https://doi.org/10.1016/j.jmatprotec.2008-04-026

[21] K.W. Wong, C.H. Shek, W. Zhang, J.K.L. Lai, σ phase dissolution in duplex stainless steel at elevated temperature studied by thermal analysis, Mater. Lett. **62** (24), 3991-3994 (2008). DOI: https://doi.org/10.1016/j.matlet.2008-05-040

[22] M. Ma, H. Ding, Z. Tang, J. Zhao, Z. Jiang, G. Li, Effect of strain rate and temperature on hot workability and flow behaviour of duplex stainless steel, Ironmaking. Steelmaking. **43** (2), 88-96 (2016).
DOI: https://doi.org/10.1179/1743281215Y.0000000053

[23] Y. Zhao, W.N. Zhang, Z.Y. Liu, G.D. Wang, Development of an easy-deformable Cr21 lean duplex stainless steel and the effect of heat treatment on its deformation mechanism, Mater. Sci. Eng. A. **702**, 279-288 (2017).
DOI: https://doi.org/10.1016/j.msea.2017-07-020

[24] S. Kleber, M. Hafok, Multiaxial Forging of Super Duplex Steel, Mater. Sci. Forum **638-642**, 2998-3003 (2010).
DOI: https://doi.org/10.4028/www.scientific.net/MSF.638-642.2998

[25] S. Kingklang, V. Uthaisangsuk, Investigation of Hot Deformation Behavior of Duplex Stainless Steel Grade 2507, Metall. Mater. Trans. A, **48**, 95-108 (2017).
DOI: https://doi.org/10.1007/s11661-016-3829-4

[26] Y.H. Yang, B. Yan, The microstructure and flow behavior of 2205 duplex stainless steels during high temperature compression deformation, Mater. Sci. Eng. A, **579**, 194-201 (2013).
DOI: https://doi.org/10.1016/j.msea.2013-05-020

[27] L.Ch. Yang, Y.T. Pan, I.G. Chen, D.Y. Lin, Constitutive Relationship Modeling and characterization of flow behavior under hot working for Fe-Cr-Ni-W-Cu-Co Super-Austenitic Stainless Steel, Metals **5** (3), 1717 (2015).
DOI: https://doi.org/10.3390/met5031717

[28] Z.H. Gao, Z.L. Tang, S.P. Xu, G.J. Cui, Offshore steel with extra-thick A514GrQ Development, World Metals **013**, 1-5 (2011).
DOI: https://doi.org/10.28826/n.cnki.nwjsd.2011.001205

[29] J.M. Cabrera, A. Mateo, L. Lanes, J.M. Prado, M. Anglada, Modeling thermomechanical processing of austenite, J. Mater. Process. Technol. **143-144**, 403-409 (2003).
DOI: https://doi.org/10.1016/ S0924-0136(03)00441-2

[30] Z.H. Feng, J.Y. Li, Y.D. Wang, The Microstructure Evolution of Lean Duplex Stainless Steel 2101, Steel. Res. Int. **88** (12), 1700177 (2017). DOI: https://doi.org/10.1002/srin.201700177

[31] H.J. McQueen, A.S. Yue, N.D. Ryan, E. Fry, Hot working characteristics of steels in austenitic state, J. Mater. Process. Technol. **53** (1-2), 293-310 (1995).
DOI: https://doi.org/10.1016/0924-0136(95)01987-P

[32] H. Mirzadeh, A. Najafizadeh, Hot Deformation and Dynamic Recrystallization of 17-4 PH Stainless Steel, ISIJ Int. **53** (4), 680-689 (2013). DOI: https://doi.org/10.2355/isijinternational.53.680

[33] Y.V.R.K. Prasad, H.L. Gegel, S.M. Doraivelu, J.C. Malas, J.T. Morgan, K.A. Lark, D.R. Barker, Modeling of dynamic material behavior in hot deformation: Forging of Ti-6242, Mater. Trans. A. **15**, 1883-1892 (1984).
DOI: https://doi.org/10.1007/BF02664902

[34] I. Calliari, M. Breda, C. Gennari, L. Pezzato, M. Pellizzari, A. Zambon, Investigation on Solid-State Phase Transformations in a 2510 Duplex Stainless Steel Grade, Metals **10** (7), 967 (2020).
DOI: https://doi.org/10.3390/met10070967

[35] N. Pettersson, R.F.A. Pettersson, S. Wessman, Precipitation of Chromium Nitrides in the Super Duplex Stainless Steel 2507, Metall. Mater. Trans. A. **46**, 1062-1072 (2015).
DOI: https://doi.org/10.1007/s11661-014-2718-y

[36] H.R.R. Ashtiani, M.H. Parsa, H. Bisadi, Constitutive equations for elevated temperature flow behavior of commercial purity aluminum, Mater. Sci. Eng. A. **545**, 61-67 (2012).
DOI: https://doi.org/10.1016/j.msea.2012-02-090